N92-21909

ISSUES IN THE ANALYSIS AND INTERPRETATION OF CYCLOTRON LINES IN GAMMA-RAY BURSTS

D. Q. LAMB
Department of Astronomy and Astrophysics and Enrico Fermi Institute
University of Chicago, 5640 S. Ellis Avenue, Chicago, IL 60637

ABSTRACT

We discuss the Bayesian approach to establishing the existence of lines, the importance of observing multiple cyclotron harmonics in determining physical parameters from the lines, and evidence from cyclotron lines of neutron star rotation.

I. INTRODUCTION

Gamma-ray bursts continue to confound astrophysicists nearly a quarter of a century after their discovery. The challenge of deciphering their nature is exacerbated by the fact that one cannot predict when or from where the bursts will occur, and the fact that it has been impossible to date to find quiescent counterparts of the bursts at radio, infrared, optical, ultraviolet, X-ray, or γ-ray energies. The latter puts a premium on garnering knowledge from the bursts themselves.

The shape of the continuum spectrum can provide important constraints on theory, but inverting it uniquely to determine the radiation mechanism, let alone physical parameters like the density and temperature, is exceedingly difficult. In contrast, the power of lines is well known: Analyses of atomic lines transformed astronomy into astrophysics. Because atomic lines are unavailable above ~ 7 keV, studies of γ-ray bursts must rely on cyclotron and, possibly, pair annihilation lines.

Gamma-ray bursts offer a particularly promising opportunity to study cyclotron lines because the bursts are bright and their X-ray continuum spectra are unusually hard. As a result, the locations, strengths, and widths of several harmonics may often be measured. This contrasts with, *e.g.*, accretion-powered pulsars, whose continuum spectra fall rapidly, even exponentially, above $\sim 20 - 30$ keV, making it difficult to detect, let alone measure the properties of, higher harmonics. Comparison of Figure 1, which shows the observed count rate and best-fit theoretical photon number spectra for the accretion-powered pulsar X0115+634, and Figure 2, which shows the same spectra for the γ-ray burst GB880205, illustrates this point.

Observations using the Los Alamos/ISAS burst detector on the *Ginga* satellite have demonstrated the existence of statistically significant harmonically spaced line features in three γ-ray bursts: GB870303 (Graziani *et al.* 1991), GB880205 (Fenimore *et al.* 1988), and GB890929 (Yoshida *et al.* 1992). Radiation transfer calculations have shown that cyclotron resonant scattering in a strong magnetic field can account quantitatively for the positions, strengths, and widths of these lines (Lamb *et al.* 1989; Wang *et al.* 1989). The success of this model convincingly demonstrates the existence of a strong magnetic field ($B \approx 2 \times 10^{12}$

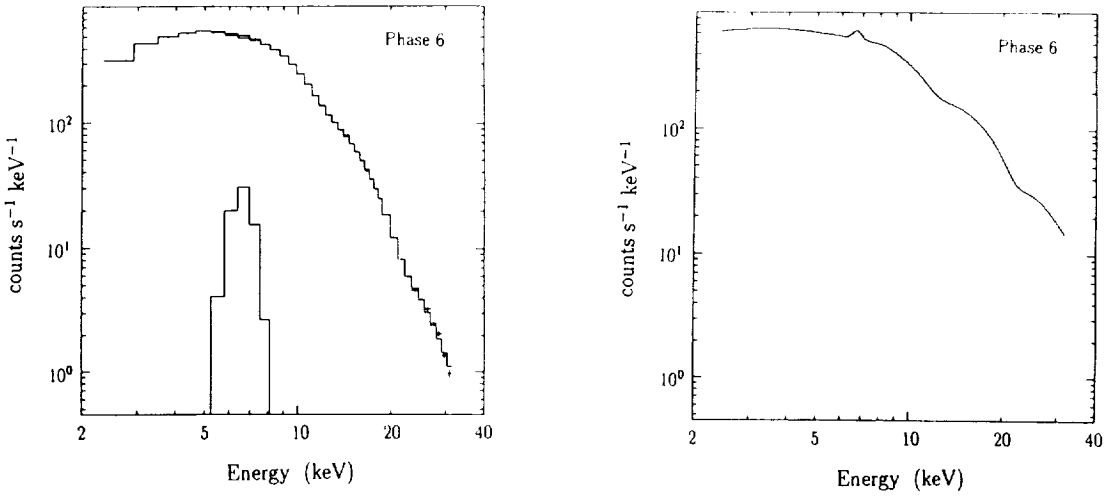

Fig. 1—*Ginga* Large Area Counter observation of the accretion-powered pulsar X0115+634 at phase 6 of the pulse. Left panel: Count rate spectrum (crosses), normalized to the width of the detector energy loss channels and best-fit theoretical count rate spectrum (histogram) and iron line contribution (narrow histogram). Right panel: Best-fit theoretical photon number spectrum. Note the cyclotron scattering lines at $\approx$ 12 and 24 keV. (After Nagase *et al.* 1991.)

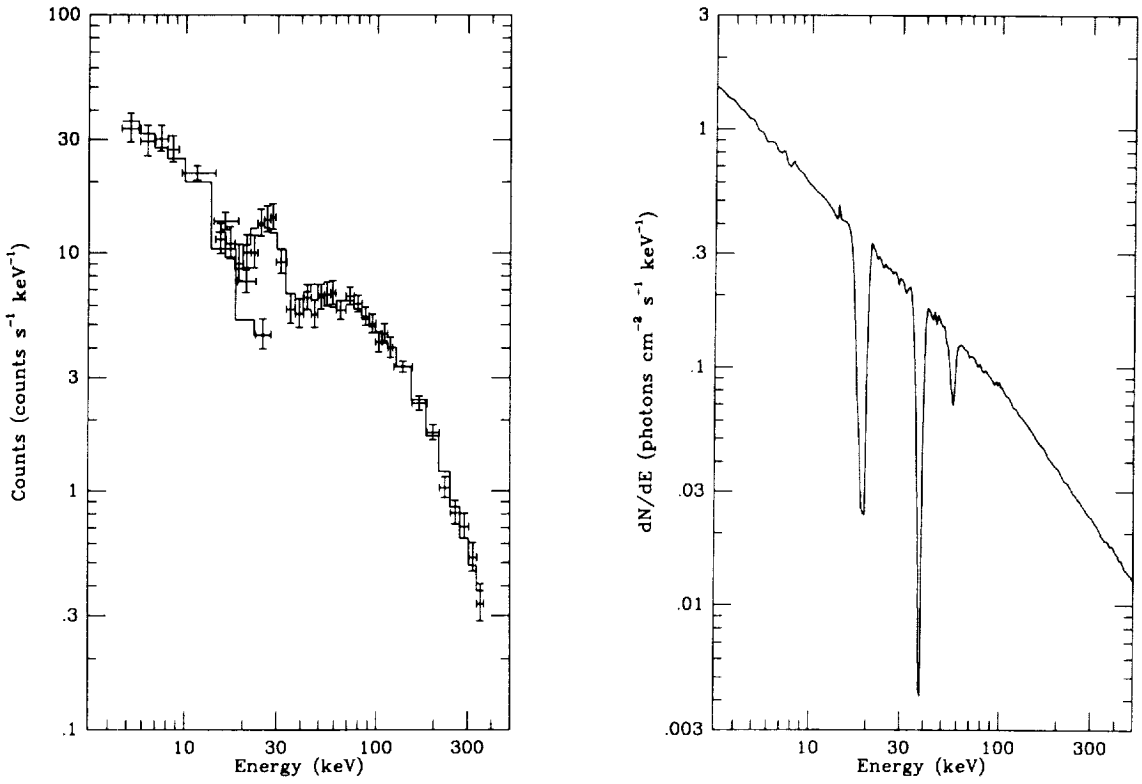

Fig. 2—*Ginga* Gamma-Ray Burst Detector spectrum of the γ-ray burst GB880205, during the 5 second interval labeled (b) in Figure 2 of Murakami *et al.* (1988). Left panel: Count rate spectra (crosses), normalized to the width of the detector energy loss channels and best-fit theoretical count rate spectra (histograms) for the PC and SC. Right panel: Best-fit theoretical photon number spectrum. Note the cyclotron scattering lines at $\approx$ 20 and 40 keV. (After Murakami *et al.* 1988 and Wang *et al.* 1989.)

G) in the sources of these γ-ray bursts. This result, taken together with the *Ginga* (Yoshida *et al.* 1991) and Konus (Mazets *et al.* 1981) data, which show low-energy lines in $\approx 15\%$ of all classical γ-ray bursts, provides compelling evidence that many γ-ray bursts come from strongly magnetic neutron stars in the Galaxy. These conclusions take on added significance with the discovery that even faint γ-ray bursts are distributed isotropically on the sky (Fishman *et al.* 1991), and the ensuing debate about whether some, or all, γ-ray bursts are cosmological in origin.

Here we explore issues in the analysis and interpretation of cyclotron lines in the spectra of γ-ray bursts; in particular, we discuss the Bayesian approach to establishing the existence of lines, the importance of observing multiple cyclotron harmonics in determining physical parameters from the lines, and evidence from cyclotron lines of neutron star rotation.

II. MODEL COMPARISON

One of the most important, yet nettlesome, issues in the analysis of cyclotron lines in γ-ray bursts is establishing the existence of the lines themselves. Here we describe a rigorous method derived from Bayesian inference; our presentation closely follows Loredo (1992; for discussions of the conceptual and methodological advantages of the Bayesian approach, see Loredo 1990).

In Bayesian inference, the probability for a model as a whole is the product of a prior probability and a global likelihood. In the absence of any information suggesting otherwise, we take the prior probabilities of competing models to be equal. Then the odds ratio in favor of one model over another is given by the ratio of their global likelihoods. Suppose that model 1 has M_1 parameters, denoted A_α, and has a minimum χ^2 equal to $\chi^2_{1,\min}$. Suppose model 2 has M_2 parameters, denoted A'_α, and has a minimum χ^2 equal to $\chi^2_{2,\min}$. Assuming Gaussian errors, the odds ratio in favor of model 2 over model 1 is,

$$O_{21} = e^{\Delta\chi^2/2}(2\pi)^{(M_2-M_1)/2}\sqrt{\frac{detV_2}{detV_1}}\frac{\prod_{\alpha=1}^{M_1}\Delta A_\alpha}{\prod_{\alpha=1}^{M_1}\Delta A'_\alpha}\,, \tag{1}$$

where $\Delta\chi^2 = \chi^2_{1,\min} - \chi^2_{2,\min}$, V_1 and V_2 are the covariance matrices for the estimated parameters, and ΔA_α and $\Delta A'_\alpha$ are the prior uncertainties for the parameters A_α and A'_α. An interesting special case of model comparison is the case of *nested models*, where one model is a special case of a more complicated model when the additional parameters in the more complicated model take on some default value (often zero). Line detection is an example of this kind of comparison: we want to compare a model consisting only of a continuum spectrum to a model with an additional feature in it. Figure 3 illustrates the simple case of a Gaussian line, where the extra parameters are the centroid energy E, the strength A, and the width ΔE of the line.

Suppose that there are C continuum parameters common to both models, and that model 2 is the larger model with L extra parameters. If the common parameters are measured with about the same precision by both models and the extra parameters are only weakly correlated with the common parameters, $\det V_2 \approx \det V_C \det V_L \approx \det V_1 \det V_L$, where V_C is the covariance matrix of the parameters common to models 1 and 2, and V_L is

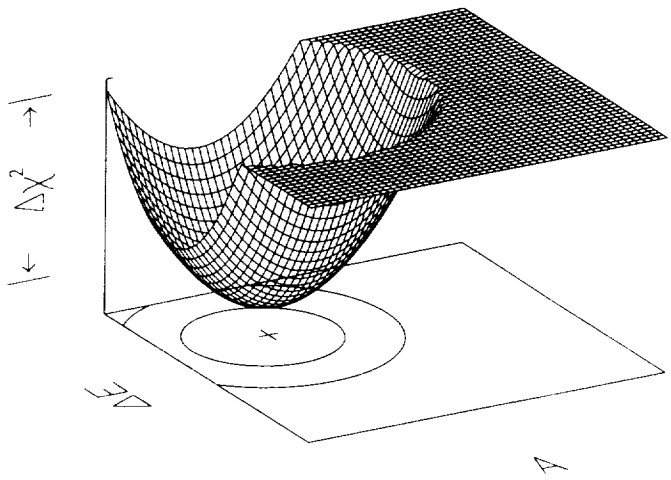

Fig. 3—χ^2 surface for two of the three additional parameters (line centroid energy E, strength A, and width ΔE) required to describe a line feature in the spectrum. The cross and the two contours in the (A,ΔE)-plane show the best-fit values of A and ΔE, and the boundaries of the 68% and 95% confidence regions for the model with a line. The vertical axis corresponds to a model with no line. $\Delta\chi^2$ is the difference in χ^2 between the best-fit theoretical models without and with a line.

the covariance matrix of the extra parameters in model 2. Further, if the covariance matrix V_L is diagonal its eigenvalues are σ_L^2, the variances for the extra parameters A'_L of model 2. Substituting these results in equation (1) gives,

$$O_{21} \approx e^{\Delta\chi^2/2} \prod_{\alpha=C+1}^{C+L} (2\pi)^{1/2}(\sigma_\alpha/\Delta A'_\alpha) \; . \tag{2}$$

Equation (2) reveals the odds ratio to be the product of the maximum likelihood ratio and a factor which includes the ratio of the posterior uncertainty of the extra parameters to their prior uncertainty. The maximum likelihood ratio will always favor the more complex model, since χ^2 of the more complex model can never be larger than that of the simpler model and therefore $\Delta\chi^2 \geq 0$. But the second factor penalizes the larger model, since the posterior uncertainty for the extra parameters will generally be smaller than their prior uncertainty. Thus an "Ockham's Razor" automatically appears in Bayesian model comparison (the dependence of this factor on the prior range superficially resembles correcting a frequentist statistic for the number of parameter values examined, but the horrendous problems associated with choosing the number and location of the examined values are absent in the Bayesian approach). Thus $\Delta\chi^2$ must exceed some critical value before the more complex model is favored.

Equation (2) also suggests an appealing intuitive connection between model comparison and parameter estimation. The quantity $\chi^2_{1,\rm min}$ corresponds to χ^2_2 minimized with respect to the common parameters, with the extra parameters fixed at their default values (*i.e.*, E arbitrary and $A = \Delta E = 0$ in the case of a simple Gaussian line; see Figure 3). But the boundary of a credible region for a subset of L parameters of a model is given by a surface of constant $\chi^2 = \chi^2_{\rm min} + \Delta\chi^2$, with $\Delta\chi^2$ chosen from the χ^2 distribution with L degrees of freedom. Thus $\Delta\chi^2 = \chi^2_{1,\rm min} - \chi^2_{2,\rm min}$ defines the boundary of a credible region for model 2 that just includes model 1 on its boundary. We can thus interpret equation (2) as stating that the data favor the more complex model (the odds ratio exceeds unity) only when the credible region that just includes the simpler model is larger than some critical size. This

critical value is

$$\Delta\chi^2 = 2\log \prod_{\alpha=C+1}^{C+L} \frac{\Delta A'_\alpha}{(2\pi)^{1/2}\sigma_\alpha} . \tag{3}$$

These results can be extended in a straightforward way to include the case of time-dependent lines. As do all Bayesian model comparisons, this case requires the explicit specification of two or more alternative models. To the extent that these models involve timescale parameters, Ockham factors will arise which penalize complicated models.

Thus Bayesian inference offers a rigorous method of establishing the existence of spectral lines which holds great promise for the analysis of γ-ray bursts.

III. PHYSICS OF CYCLOTRON SCATTERING

Cyclotron *resonant scattering*, in which electrons undergo radiative $0 \rightarrow 1 \rightarrow 0$ Landau transitions, produces a dip at the first harmonic frequency $\omega \approx \omega_B$. No simple description can be used to explain the first harmonic line, whose appearance depends critically on the outcome of the multiple resonant scatters required in order for individual photons to escape (Wang, Wasserman, and Salpeter 1988), as well as on the introduction of new photons at energies near that of the first harmonic which are "spawned" by Raman scattering at the higher harmonics, as described below.

Resonant Raman scattering, in which electrons undergo $0 \rightarrow n \rightarrow n-1 \rightarrow ... \rightarrow 1 \rightarrow 0$ radiative transitions, produces dips at the second and higher harmonics ($\omega \approx N\omega_B$). Resonant scattering of second and higher harmonic photons, in which electrons undergo radiative Landau transitions in which $\Delta n > 1$ (*i.e.*, $0 \rightarrow 2 \rightarrow 0$) are rare because $B/B_c \ll 1$. Because most of the photons which undergo scattering at the second and higher harmonics are destroyed, the resulting line feature is approximately that for absorption.

Figure 4 shows theoretical photon number spectra for two different viewing angles θ relative to the magnetic field. The bottom and middle lines show the line profiles that would result, were they due to absorption, and resonant and Raman scattering without photon spawning, respectively. The (heavy) top line gives the actual line profiles, which are due to resonant scattering and Raman scattering with photon spawning. Figure 4 shows that the strengths of the first and second harmonic lines are comparable. Figure 4 also shows that the profiles of the second and third harmonics closely resemble those for absorption and are asymmetric due to relativistic kinematics in one dimension.

The resonant scattering cross section at the $N^{\rm th}$ harmonic is $\propto (1+\cos^2\theta)\sin^{2N-2}\theta$. Thus scattering of photons at the first harmonic is moderately peaked along the magnetic field, while scattering at higher harmonics is strongly peaked away from the magnetic field. Therefore Raman scattering primarily removes photons traveling perpendicular to the magnetic field. However, the photons spawned at the first harmonic by resonant Raman scattering at higher harmonics are created with the angular distribution characteristic of the first harmonic, and therefore have an angular distribution moderately peaked along the magnetic field. In scattering, a photon undergoes on average a relative shift in frequency $\approx (v_{th}/c)\cos\theta$ due to the thermal motion of the electrons along the magnetic field. Therefore the Doppler width of the cyclotron lines is large looking along the magnetic field

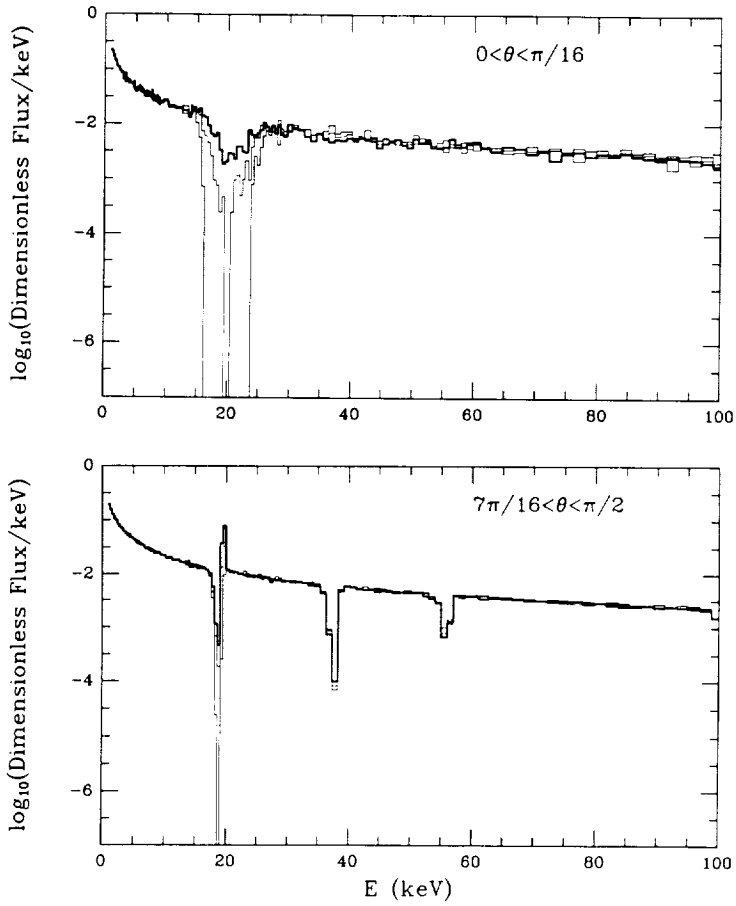

Fig. 4—Theoretical photon number spectra for $B = 1.71 \times 10^{12}$ G, $N_e = 1.2 \times 10^{21}$ electrons cm^{-2}, $T = 5.3$ keV, and two different viewing angles θ relative to the magnetic field. The bottom and middle lines show the line profiles that would result from absorption, and resonant and Raman scattering without photon spawning. The (heavy) top line gives the actual profiles, which are due to resonant scattering, and Raman scattering with photon spawning. (From Lamb, Wang, and Wasserman 1991.)

and decreases as one looks away from it. Figure 4 shows that these two effects produce pronounced variations in the strengths and widths of the various harmonics as a function of viewing angle θ.

IV. PARAMETER ESTIMATION

Observations using the Los Alamos/ISAS burst detector on *Ginga* have demonstrated the existence of statistically significant harmonically spaced cyclotron lines in three γ-ray bursts. Analysis of these observations using radiation transfer calculations have shown that cyclotron resonant scattering in a strong magnetic field can account quantitatively for the positions, strengths, and widths of these lines. Here we emphasize that the power of this analysis depends crucially on the observation of *multiple* lines.

As described in the previous section, the relative strengths of the first and higher harmonics show a pronounced variation with viewing angle θ: at small θ only the first harmonic is visible, while at large θ the second harmonic is dominant (see Figure 4). This is particularly the case for current detectors, which effectively integrate over the scattering dip and the spawned photon peak at the first harmonic because of modest spectral resolution. As a result, if we observe one line only, we have no way of knowing whether this line corresponds to the first or second harmonic. Obviously, the value of the magnetic field will be uncertain by a factor of two (as in, *e.g.*, the Konus bursts).

TABLE 1
BEST-FIT MODEL PARAMETERS

Line Parameters	Absorption Model	Scattering Model
B (10^{12} G)	1.69 ± 0.04	1.71 ± 0.07
N_e (10^{21} cm^{-2})	—	1.2 ± 0.6
$\mu(=\cos\theta)$	—	0.31 ± 0.05
$kT_{\parallel}\cos^2\theta$ (keV)	6.6 ± 2.4	—
$N_{e,1}^{los}(1+\cos^2\theta)$ (10^{21} cm^{-2})	≈ 0.23	—
$N_{e,2}^{los}(1-\cos^4\theta)$ (10^{21} cm^{-2})	≈ 2.4	—

Worse, however, is the fact that analysis of the line cannot determine the physical parameters of the line-forming region, *i.e.*, its optical depth (or column density), temperature (or velocity), and the geometry (or viewing angle). This is because the physics of the line formation is very different for the first and second harmonics; without knowing which harmonic we are observing, we do not know which physics to apply. Even if we somehow knew which harmonic we are observing, analysis of a single cyclotron line cannot determine the physical parameters of the line-forming region. This is because the line is a function of four parameters (the magnetic field strength B, the temperature T and column depth N_e of the line-forming region, and the viewing angle θ), but current detectors are sensitive only to two (*e.g.*, the centroid energy E and the equivalent width EW) because of modest spectral resolution. As a result, a single line can be fit by an infinite family of solutions in which N_e decreases and T increases as θ increases.

This situation is illustrated by the cyclotron absorption model, which has been used by many authors. The choice of this model is motivated by the facts that the model is analytic and that approximating cyclotron Raman scattering by cyclotron absorption is valid at higher harmonics. However, such an approximation is not valid at the first harmonic, and therefore *different temperatures and column densities must be allowed at the first and second harmonics.* The situation then becomes equivalent to fitting a single line, even if the first and second harmonic are both strongly present.

The free parameters of the cyclotron absorption model are then the line centroid energies $E_1 = E_2$, the line widths $\Delta E_N = E_N(2kT_{\parallel}\cos^2\theta/mc^2)$, where θ is the viewing angle relative to the magnetic field, and the line strengths $A_N = N_{e,N}^{los}\alpha_N$, where $N_{e,N}^{los}$ and α_N are the column density along the line of sight and the absorption coefficient of the N^{th} harmonic. The physical parameters that may be deduced from the fit are $N_{e,1}^{los}(1+\cos^2\theta)$ and $N_{e,2}^{los}(1-\cos^4\theta)$, and $kT_{\parallel,1}\cos^2\theta/mc^2$ and $kT_{\parallel,2}\cos^2\theta/mc^2$. However, $N_{e,1}^{los}$ and $kT_{\parallel,1}\cos^2\theta/mc^2$ have no straightforward physical meaning because the cyclotron absorption model is not valid at the first harmonic, respectively. Table 1 gives the best-fit parameters of the model for GB880205 (Fenimore *et al.* 1988); as expected, B is well-determined but θ is undetermined and T and $N_e^{\rm los}$ are therefore poorly constrained.

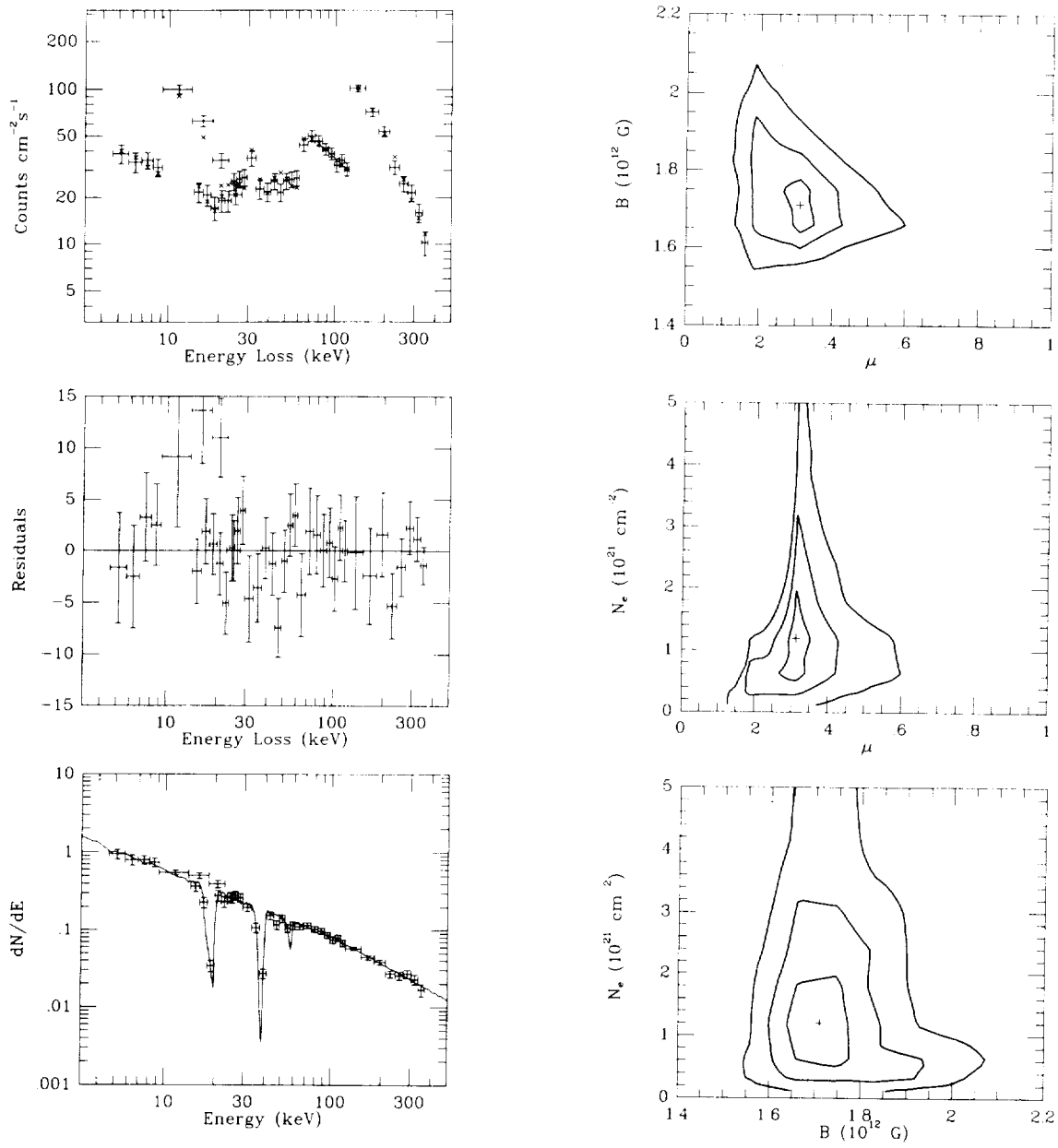

Fig. 5—(top) Observed (crosses) and best-fit theoretical (x's) count rate spectrum of the proportional counter (PC) and scintillation counter (SC) on *Ginga* for GB880205. (middle) Residuals for the PC and SC counters. (bottom) Best-fit theoretical photon number spectrum (solid curve) and *Ginga* PC and SC data (crosses). (From Wang *et al.* 1989.)

Fig. 6—The 68.3%, 95.4%, and 99.7% confidence regions in (B, N_e, μ)-space, as determined by χ^2 fits of theoretical photon number spectra to the *Ginga* data for GB880205: (top) projected in the (μ, B)-plane; (middle) projected in the (μ, N_e)-plane; (bottom) projected in the (B, N_e)-plane. (From Wang *et al.* 1989.)

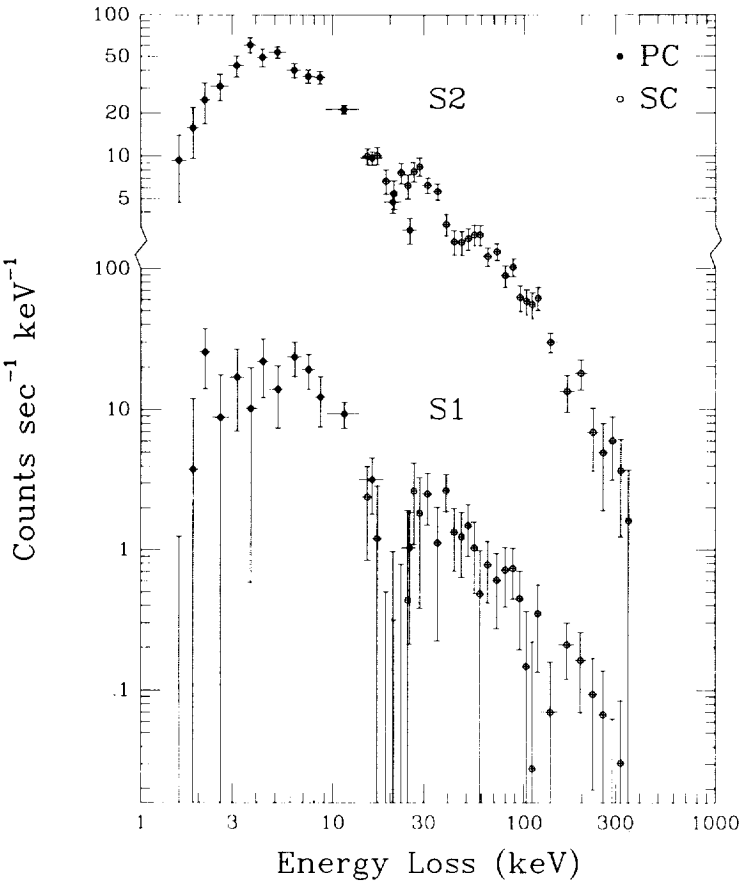

Fig. 7—Count rate spectra for intervals S1 and S2 of GB870303, normalized by energy bin width, for the proportional counter (PC) and scintillation counter (SC) on *Ginga*. Note the strong dip at $\approx$ 20 keV in S1 and the dips at $\approx$ 20 and 40 keV in S2. (From Graziani *et al.* 1991.)

In contrast, if *multiple lines* are strongly present, the physical parameters B, N_e, kT, and θ can be determined.

If only the first and second harmonics are present, theoretical radiation transfer calculations are required. This approach is illustrated by the fits to the spectrum of GB880205 carried out by Wang *et al.* (1989). Folding Monte Carlo spectra through the *Ginga* detector response functions, they fit the observed photon count rate spectrum. Figure 5 shows the predicted and observed photon count-rate spectra, the residuals, and the incident photon-number spectrum for the best-fit parameters. Figure 6 shows the 68.3%-, 95.4%-, and 99.7%-confidence regions in (B, N_e, μ)-space. Table 1 gives the best-fit parameters of the model. The resonant cyclotron Compton temperature is not a free parameter, but is fixed by their model to be $T_C = 5.3^{+0.3}_{-0.2}$ keV.

If multiple higher harmonic lines are strongly present, one has three observed quantities ($E_1 = 2E_2$, EW_1, and EW_2) and some information about two others (ΔE_1 and ΔE_2) to determine the four physical parameters (B, T, N_e or $N_e^{\rm los}$, and θ). The physical parameters can then be determined using either the absorption model or theoretical radiation transfer calculations. However, multiple higher harmonic lines will be strongly present only if the column density of the line-forming region is large. To date, such column depths have not been seen in γ- ray bursts.

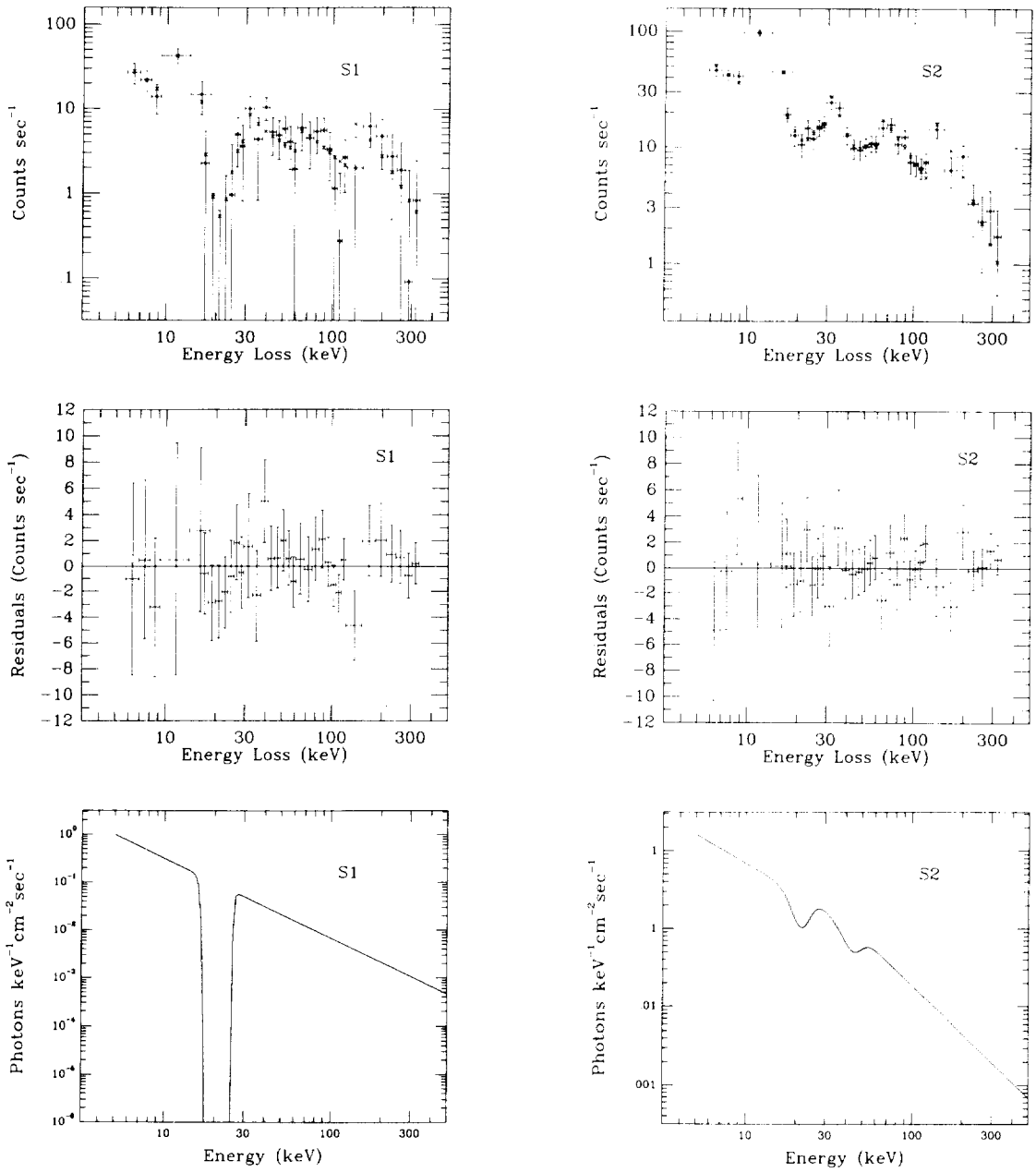

Figure 8—(top) Observed count-rate spectra (+'s) and best-fit absorption model count-rate spectra (x's) for intervals S1 and S2 of GB870303 for the PC and SC data on *Ginga*. (middle) Residuals. (bottom) Best-fit absorption model photon-number spectra. (From Graziani *et al.* 1991.)

V. NEUTRON STAR ROTATION

The pronounced variations in the strengths and widths of the cyclotron lines as a function of θ provide *a distinct signature of neutron star rotation.* As a simple example, consider cyclotron lines formed in a small region near one magnetic pole of an orthogonally rotating neutron star with the observer located in the plane perpendicular to the rotation axis. Then the rotation angle $\phi = \theta$. As the neutron star rotates, θ varies, producing

TABLE 2
BEST-FIT ABSORPTION MODEL PARAMETERS

Line Parameters	S1	S2
E_1 (keV)	$21.1^{+1.1}_{-1.0}$	21.4 ± 0.7
$kT_1 \| \cos^2\theta$ (keV)	< 15	$8.18^{+7.15}_{-4.29}$
$N^{los}_{e,1}(1+\cos^2\theta)$ (cm^{-2})	$> 3.14 \times 10^{20}$	$(1.19^{+0.23}_{-0.20}) \times 10^{20}$
$kT_2 \| \cos^2\theta$ (keV)	—	$10.5^{+10.5}_{-5.77}$
$N^{los}_{e,2}(1-\cos^4\theta)$ (cm^{-2})	—	$(2.33^{+0.48}_{-0.45}) \times 10^{21}$
EW_1 (keV)	10.5 ± 2.1	$4.81^{+0.90}_{-0.82}$
EW_2 (keV)	—	$8.45^{+0.26}_{-0.21}$

pronounced variations in the strengths and widths of the cyclotron lines. Looking down the magnetic field ($\theta = 0$), the first harmonic is strong and wide, due to Doppler broadening, but no higher harmonics are visible. As the viewing angle θ increases, the strength of the first harmonic decreases while the strengths of the higher harmonics, particularly the second, increase. At the same time, the Doppler widths of all the lines decrease. Figure 4 illustrates this behavior.

While such a combination of variations in line strengths and widths may not be unique, simple changes in the temperature or column depth of the line-forming region do not suffice to produce it. A decrease in the temperature produces narrower lines, but does not change the strength of the first harmonic relative to the higher harmonics. A decrease in the column depth of the line-forming region produces a weaker first harmonic, but also produces weaker, not stronger, higher harmonics.

Graziani *et al.* (1991) find that the burst GB870303 exhibits two broad peaks and lasts approximately 45 sec. An exhaustive search of the data revealed two time intervals (hereafter S1 and S2) in which statistically significant spectral lines are seen. S1 is a previously unreported 4 sec interval; S2 is the 9 second interval reported in Murakami *et al.* (1988). The midpoints of S1 and S2 are separated by 22.5 sec. Figure 7 shows the count rate spectra for S1 and S2, normalized to the width of the energy loss channels; the spectrum for S2 is identical to that reported in Murakami *et al.* (1988). Note the line at $\approx$ 20 keV in the S1 spectrum, and the two lines at $\approx$ 20 and 40 keV in the S2 spectrum.

Graziani *et al.* (1991) carried out a one-line (3-parameter) fit to S1 and a separate two-line (5-parameter) fit to S2, using the cyclotron absorption model. Figure 8 shows the observed count-rate spectra (+'s) and best-fit absorption model count-rate spectra (x's) for S1 and S2. Also shown are the residuals and the best-fit absorption model photon-number spectra. Table 2 gives the best-fit parameters and 1σ errors for the absorption model fits to S1 and S2. The values of $kT_\parallel \cos^2\theta/mc^2$ and $(\rho h)_1(1+\cos^2\theta)$ for S1 are only upper and lower 95% confidence limits, respectively, because the line feature is so deep that, after background subtraction, the net counts in some channels are negative,

although the error bars extend to positive values. Thus the fit can always be made slightly better by increasing β_1 and compensating by decreasing ΔE_1. Table 2 implies very similar magnetic field strengths for S1 and S2: $B = (1.82^{+0.095}_{-0.086}) \times 10^{12}$ G and $(1.86 \pm 0.06) \times 10^{12}$ G, respectively. Table 2 also shows that the Doppler widths of the first and second harmonics are similar for S1 and S2, within statistical uncertainties; in contrast, the strengths (and EW) of the first and second harmonics differ greatly for the two intervals.

Comparison of Figures 4 and 8 shows that the change in the line spectrum between S1 and S2 is qualitatively similar to that produced by a change in the viewing angle θ. We conjecture that this change is due to rotation of the neutron star. We suggest that during S1 our line of sight is nearly parallel to the field, so that only the first harmonic is visible, while during S2 our line of sight is nearly perpendicular to the field, so that both first harmonic and second harmonics are visible, with comparable strengths (see Figure 4). The time Δt between the centers of S1 and S2 is 22.5 sec. Within the framework of the rotation picture, we may associate Δt with either a minimum change in rotational phase $\Delta\phi \approx \pi/4$ or a maximum change $\Delta\phi \approx \pi$. These values constrain the rotation period P of the neutron star to lie in the range 2×22.5 sec ≈ 45 sec $\lesssim P \lesssim 8 \times 22.5$ sec ≈ 180 sec.

This result, if confirmed, has profound implications for the location, extent, and stability of the γ-ray burst line-forming region, and for the origin and evolution of the magnetic neutron stars which are the sources of many γ-ray bursts.

We gratefully acknowledge the contributions of our collaborators, particularly Ed Fenimore, Tom Loredo, Toshio Murakami, John Wang, Ira Wasserman, and Atsumasa Yoshida, to the work described here. This work was supported in part by NASA grants NAGW-830 and NAGW-1284.

REFERENCES

Fenimore, E. E. *et al.* 1988, *Ap. J. Lett.*, **335**, L71.

Fishman, G. J., *et al.* 1991, these proceedings.

Graziani, C., *et al.* 1991, in *Proceedings of the Taos Workshop on Gamma-Ray Bursts*, ed. C. Ho, R. I. Epstein, and E. E. Fenimore (Cambridge U. Press: Cambridge), p. 407.

Lamb, D. Q., *et al.* 1989, *Ann. NY Acad. Sci.*, **571**, 460.

Lamb, D. Q., Wang, J. C. L., and Wasserman, I. 1990, in *Proceedings of the Taos Workshop on Gamma-Ray Bursts*, ed. C. Ho, R. I. Epstein, and E. E. Fenimore (Cambridge U. Press: Cambridge), p. 415.

Loredo, T. J. 1990, in *Maximum Entropy and Bayesian Methods*, ed. P. F. Fougère (Dordrecht: Kluwer Academic Publishers), p. 81.

Loredo, T. J. 1992, in preparation.

Mazets, E. P., *et al.* 1981, *Nature*, **290**, 378.

Murakami, T. *et al.* 1988, *Nature*, **335**, 234.

Nagase, F., *et al.* 1991, ISAS Report No. 476.

Wang, J. C. L. *et al.* 1989, *Phys. Rev. Lett.*, **63**, 1550.

Wang, J. C. L., Wasserman, I., and Salpeter, E. E. 1988, *Ap. J. Suppl.*, **68**, 735.

Yoshida, A., *et al.* 1991, *Pub. Astron. Soc. Japan*, in press.